Chalcogenide Letters Vol. 17, No. 4, April 2020, p. 179 - 186

STRUCTURAL, OPTICAL AND ELECTRICAL PROPERTIES OF Cu_2NiSnS_4 THIN FILMS DEPOSITED BY CHEMICAL SPRAY PYROLYSIS METHOD

M. A. ABED[a,b], N. A. BAKR[a,*], J. AL-ZANGANAWEE[a]
[a]*Department of Physics, College of Science, University of Diyala, Diyala, Iraq*
[b]*Diyala Directorate General of Education, Diyala, Iraq*

In this study, Cu_2NiSnS_4 (CNTS) thin films were deposited on glass substrates at different temperatures of 250, 300, 350 400, and 450 ˚C using the chemical pyrolysis technique. The aim of this research was to study the effect of the substrate temperature on the properties of the films. The structural properties of the films were obtained by X-ray diffraction, Raman spectroscopy, and Field Emission Scanning Electron Microscopy (FESEM); the optical properties were determined by the UV-Vis spectroscopy; and the electrical properties were obtained by observing the Hall Effect. The XRD results showed that the CNTS films had a cubic crystalline structure with (111) being the preferred and most common orientation plane. Raman spectroscopy results showed a distinct peak at 336 cm^{-1}, which indicated a CNTS quaternary compound. The FESEM results demonstrated the presence of nanoparticles with various shapes and sizes. The optical energy band gap was proven to have a value of 1.57-1.82 eV, for the allowed direct transition, and a high absorption coefficient ($\geq 10^4$ cm^{-1}) in the visible spectrum region, thereby indicating the potential application of these thin films in solar cells. The Hall Effect measurement on the CNTS thin films indicated a p-type of conductivity for all films, with the highest charge carrier density and mobility occurring at 350˚C, which makes them ideal for use in photovoltaic applications.

(Received November 13, 2019; April 3, 2020)

Keywords: Cu_2NiSnS_4 thin films, Chemical spray pyrolysis, Substrate temperature, Structural properties, Optical properties, Hall effect

1. Introduction

Recently, combinations of quaternary chalcogenides of Cu_2MSnS_4 (M= Ni, Fe, Mn, Zn) have attracted wide attention because they are regarded as absorbent layers with distinctive chemical, electrical and optical characteristics in thin-film solar cells. The Cu_2NiSnS_4 thin film is one such promising film for solar cell device because it has a suitable band gap energy (1.5-1.8 eV) and high optical absorption coefficient (about $\geq 10^4 cm^{-1}$) [1, 2]. A few studies have been carried out on the composition of CNTS thin films. N. Bitri et al. manufactured a cubic-structured CNTS thin film without any heat treatment using the Spray Sandwich technique [1]. Yang et al. studied the stannite structure of CNTS thin films using a facile one-step electro-deposition technique with annealing in an impure atmosphere [2]. In this study, the effect of the substrate temperature on the optical, structural and electrical properties of CNTS thin films deposited by chemical spray pyrolysis technique was systematically investigated.

2. Experimental method

The solution for the Cu_2NiSnS_4 (CNTS) thin films was prepared by dissolving $Cu_2Cl_2.2H_2O$, $NiCl_2.6H_2O$, $SnCl_2.2H_2O$, and thiourea (SC $(NH_2)_2$) at concentrations of 0.1M, 0.05M, 0.05M, and 0.4M, respectively in 100 ml of distilled water at room temperature. The concentration of thiourea was doubled to compensate the quantity evaporated due to the high temperature used for the growth of the thin films. The metal and thiourea salts were dissolved in

* Corresponding author: nabeelalibakr@yahoo.com

the assigned container with the volume of distilled water for each material, and the solution was then placed on a magnetic stirrer until a state of complete dissolution had been achieved. The prepared solutions were then filtered individually and mixed for some time in a single glass flask using a magnetic stirrer to ensure their homogeneity. Few drops of HCl acid or ethanol might be added with constant stirring into the solution for complete homogeneity. The pH value of the final solution was ~1-2. The solution was then sprayed onto glass substrates at different temperatures of 250, 300, 350, 400, and 450 $^{\circ}$C using a home-made device at constant deposition parameters, as mentioned elsewhere [3]. The solution was sprayed continuously onto the glass substrates for 10 seconds, after which, the spraying was stopped for 3 minutes to prevent over-cooling of the substrate and to allow the thickness of the thin films to reach 350±10 nm. The prepared thin films had a strong adhesion and a uniform thickness, which was measured using the gravimetric method. The synthetic properties were confirmed using X-ray diffractometer (Bruker D8 Advance, Germany) with a target CuKa (λ= 1.54056 Å) as the source. The topography of the surface of the thin film was imaged using FESEM (Nova NanoSEM FEI 450 model). The Raman spectra were recorded with a backscattering design utilizing a Jobin-Yvon Horiba Labram800. The optical properties of the prepared films were determined through the use of a Shimadzu, UV- 1800. The Hall Effect was investigated using the HMS 3000 system.

3. Results and discussion

The results of the X-ray diffraction patterns of the CNTS films prepared at different temperatures of 250, 300, 350, 400, and 450 $^{\circ}$C with a thickness of 350±10 nm, are shown in Fig. 1. The thin films had a cubic crystalline structure with the space group, (F-43m), with distinguished peaks at approximate angles of 2θ ~28.47°, 33.02°, 47.35°, 56.21°, which were achieved by the reflection of crystalline planes (111), (200), (220), and (311) respectively, belonging to the cubic CNTS compound. The secondary phases of Cu_2S, SnS, Cu_3SnS_4 were absent, and a dominant peak indicating a favoured growth at the crystalline plane of (111) [4]. These results were in agreement with the standard card number (26-0552). Table 1 shows the XRD results for the CNTS films for the prevailing growth in the direction of (111) plane.

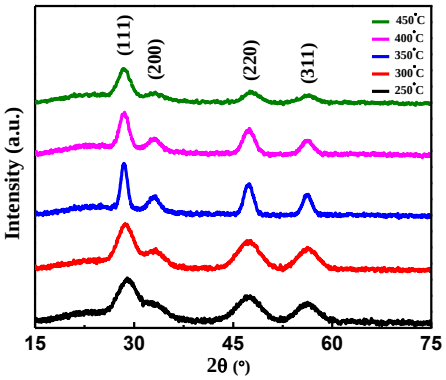

Fig. 1. X-ray diffraction patterns of CNTS thin films at different substrate temperatures.

Depending on the Bragg's equation, the formula for the inter-planar spacing was estimated by [5]:

$$d_{hkl} = \frac{a}{\sqrt{(h^2+k^2+l^2)}} \quad (1)$$

The lattice constant was determined to be equal to a = b = c = 5.423 Å, which was very close to the standard card data (a = b = c = 5.425 Å).

Table 1. Structural parameters of the XRD results of CNTS thin films at different substrate temperatures.

Substrate Temperature (°C)	2θ (deg)	d (Å)	D (nm)	Tc	Unit Cell Volume (Å^3)
250	28.82	3.095	1.680	0.59	153.99
300	28.58	3.120	2.295	0.46	157.72
350	28.48	3.131	5.791	0.49	159.48
400	28.52	3.127	3.866	0.53	158.86
450	28.38	3.142	2.804	0.54	161.16

The crystallite size (D) was calculated using Scherrer's formula for the direction (111) [5].

$$D = \frac{k\lambda}{\beta cos\theta} \tag{2}$$

where β is the FWHM of the main peak, λ is the X-ray wavelength (1.54056 Å), and k is the shape factor (k = 0.9). The results of the calculations are shown in Fig. 2 indicating that the crystallite size increased when the deposition temperature of the prepared films was increased, and began to decrease when the temperature continued to rise to more than 350 °C for the CNTS thin films. This was due to the fact that once this temperature was reached; there was excessive evaporation of the sprayed droplets before they reached the hot substrate due to the high thermal energy, which was inappropriate and larger than what was required to obtain the complete decomposition and re-crystallization of the samples. Thus, the crystallization process was incomplete [6]. The texture coefficient was studied using the following formula [7]:

$$T_C = \frac{I_{(hkl)}/I_{\circ(hkl)}}{N_r^{-1}\sum I_{(hkl)}/I_{\circ(hkl)}} \tag{3}$$

where $I_{(hkl)}$, $I_{(\circ hkl)}$ is the measured intensity and intensity of the standard card, respectively, N_r is the number of peaks shown in the X-ray diffraction pattern, and hkl are the Miller indices. The texture coefficient was calculated at the crystal plane (111) of the CNTS thin films. The calculated texture coefficient of the CNTS films was less than one, which indicates that the films were polycrystalline and had more than one growth direction.

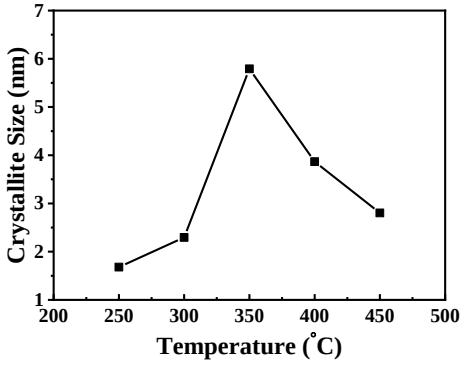

Fig. 2. Crystallite size of CNTS thin films at different substrate temperatures.

Although it was possible to identify the phase by X-ray diffraction, it was not clearly distinguishable because of the similarity of the composition between the phases of the material itself. Therefore, Raman spectroscopy measurements were made for the samples at room temperature. From the results of the Raman spectra (CNTS) shown in Fig. 3. and Table 2., the

main peak at position 336 cm^{-1} appeared to have a high and clear intensity, with the appearance of other peaks with a low intensity at the positions of 251 cm^{-1} and 178 cm^{-1}. This was in agreement with the results of previous reports [8].

Table 2. Results of Raman spectroscopy of CNTS thin films at different substrate temperatures.

Substrate Temperature (^{o}C)	Peak Center (cm^{-1})	Peak Width (cm^{-1})	Intensity (ar. u.)
250°C	336	35.68	87.72
300°C	336	30.56	90.34
	250	7.37	8.04
350°C	336	27.36	80.96
	250	6.68	11.00
	178	17.67	7.33
400°C	336	29.21	85.69
	250	7.10	9.63
	177	29.27	3.77
450°C	336	32.75	89.27
	251	6.64	3.92

The topography of the surface of the deposited thin films was studied at different substrate temperatures using FESEM technique, and was characterized by a very high magnification power and accuracy. Fig. 4 shows the microscopic images of the CNTS films with a magnification of 100 kx. It was noted from the FESEM images that irregular particle shapes with voids and cracks had been formed, where at a temperature 250 °C, the growth of particles in the form of clusters was observed due to the aggregation of particles of the material at the surface, which create areas of nucleation in this region. When the temperature was increased to 300 °C, formations, similar to nano-sheets, were lined up vertically, and at a temperature of 350 °C, the surface appeared flat with the appearance of hexagonal forms, which indicated the beginning of the formation and growth of a new layer. However, at 400 toand 450 °C, structures similar to nano paper and hexagonal nano-bars were formed, and there was evidence that confirmed the growth of a new layer, with great dominance on the surface of the film, and the formation of small pieces, which began to disappear as the temperature increased. The granules in the CNTS films were of different sizes, being about ~59 and 244 nm at 400°C and 350°C, respectively. This difference in the granular size and shapes may have been due to a lack of homogeneity in the thin films [9, 10].

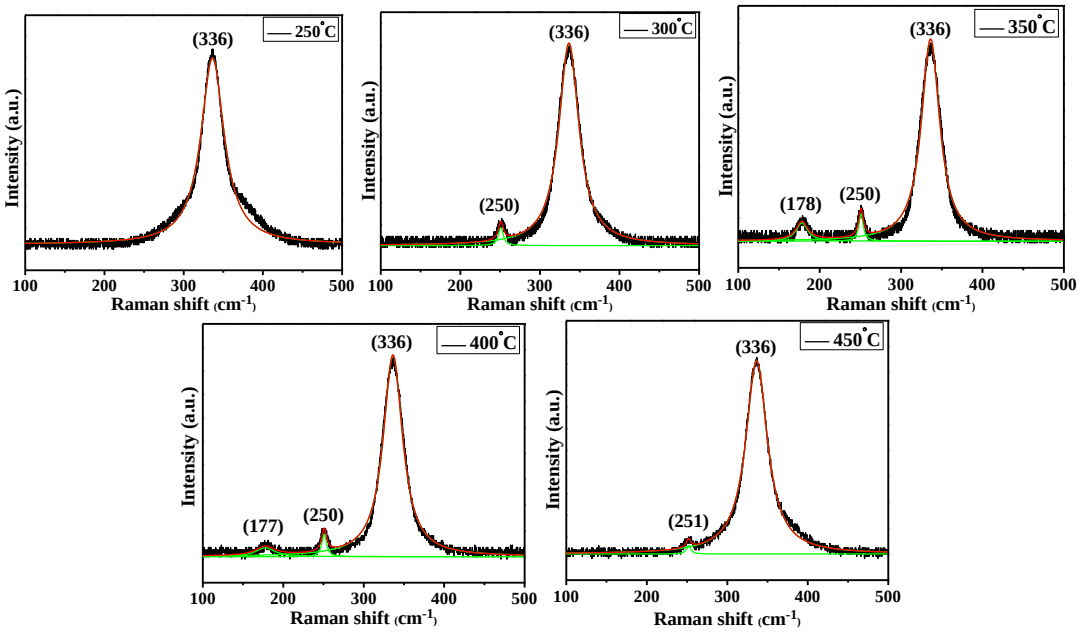

Fig. 3. Raman spectra of CNTS thin films at different substrate temperatures.

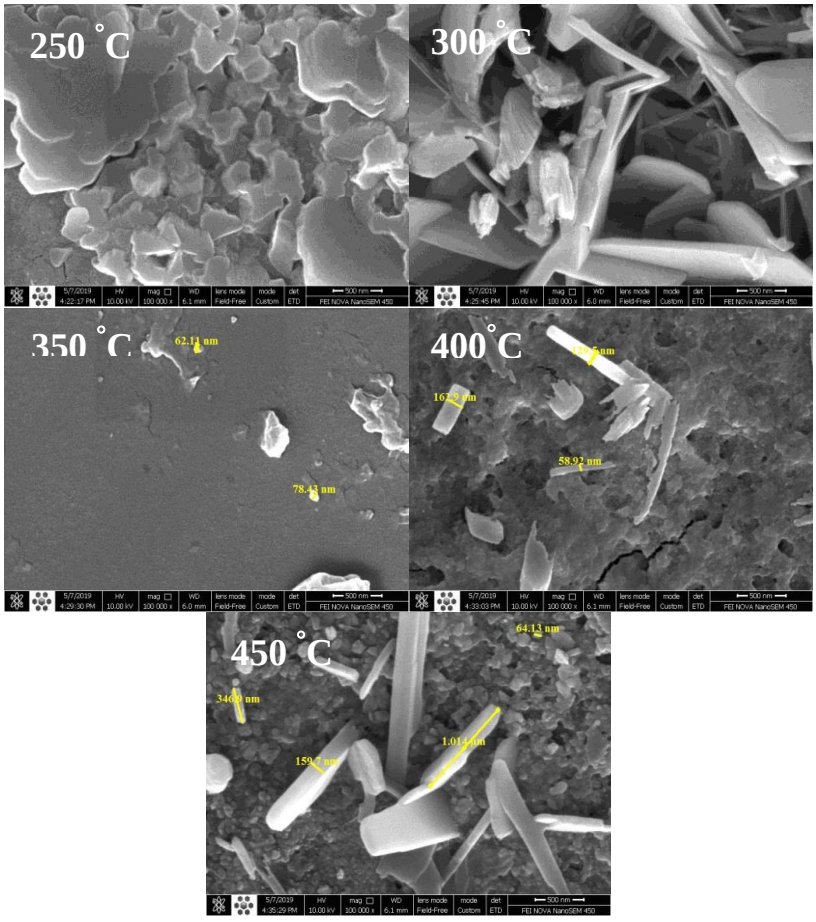

Fig. 4. FESEM micro images of CNTS thin films at different substrate temperatures.

The optical properties of the CNTS thin films were verified using the absorbance and transmittance spectra from UV-visible spectroscopy. The optical absorption coefficient was calculated using the following relationship [11]:

$$\alpha = 2.303\ A/t \tag{4}$$

where t is the thickness of the CNTS thin films, and A is the absorbance. It was found that the value of the optical absorption coefficient of the CNTS films was higher than $10^4 cm^{-1}$. The optical band gap, E_g, was calculated from the absorption spectrum using the Tauc's model, as in the relationship [11]:

$$(\alpha h\upsilon) = B(h\upsilon - E_g)^n \tag{5}$$

where B is a constant, depending on the nature of the material, E_g is the optical band gap energy, h represents Planck's constant, υ is the frequency of light, $h\upsilon$ is the photon energy, and n is an empirical index that characterizes the absorption process. The value of n depends on the electronic transition in the material, where n is 1/2, 2 and 3 for direct allowed transition, allowed transition, and direct forbidden transition, respectively. In this work, the direct band gap was determined by plotting a graph between $(\alpha h\nu)^2$ and $(h\nu)$ in eV, where a straight line was obtained. The extrapolation of this straight line to $(\alpha h\nu)^2 = 0$ gave the value of the direct band gap of the material, as shown in Fig. 5. It was found that the values of the energy gap calculated by the available results were equal to 1.57-1.82 eV, as shown in Fig. 5a and 5b. The variation in the value of the optical energy gap may have been due to the variation in the crystallite size and high density of the local states in the composition of the bands resulting from the heterogeneous stress or unsaturated bonds introduced during the chemical reaction, and this corresponded with the results of other studies [12] .

To describe the electrical properties of the CNTS thin films, the Hall Effect was measured at room temperature to determine the concentration, type, and mobility of the majority charge carriers, and the conductivity. The results of the measurements in Table 3 showed that the conductivity was of p-type, and this was in agreement with the results of the previous study [13]. It was noted from Figures 6 and 7 that the electrical conductivity, mobility and charge carriers concentration increased when the temperature of the substrate was increased up to 350°C, after which, they began to decrease, the reason being the occurrence of a more complete crystallization at this temperature. This was confirmed by the results of the X-ray diffraction [6].

Table 3. Results of Hall Effect measurements of CNTS thin films at different substrate temperatures.

Substrate Temperature ($^{\circ}$C)	R_H (cm^3/C)	n (cm^{-3})	μ ($cm^2/v.s$)	ρ (Ω.cm)	σ $(\Omega.cm)^{-1}$
250	150.76	4.14×10^{16}	24.562	6.138	0.162
300	86.33	7.23×10^{16}	29.233	2.953	0.338
350	62.86	9.93×10^{16}	44.757	1.404	0.712
400	77.34	8.07×10^{16}	38.556	2.006	0.498
450	79.71	7.83×10^{16}	32.106	2.483	0.402

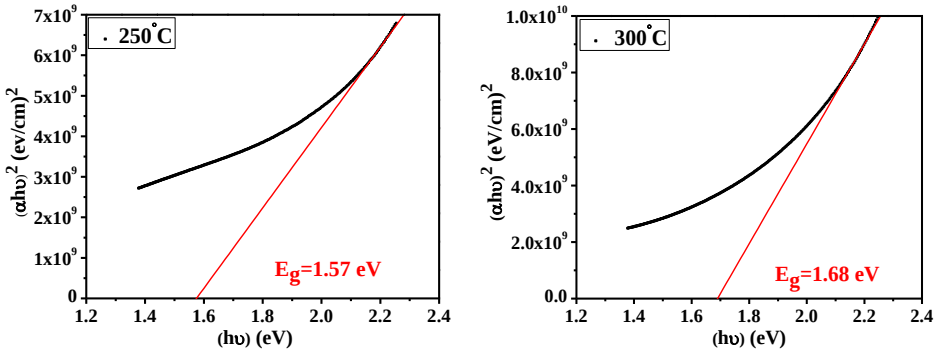

Fig. 5 a. Tauc's plots of CNTS thin films at 250 °C and 300 °C.

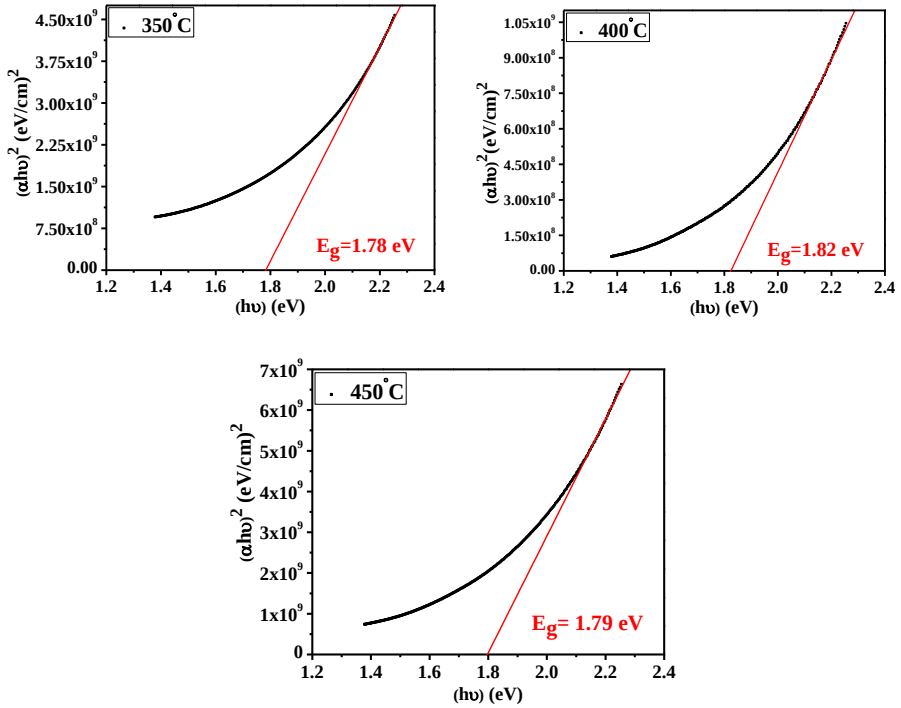

Fig. 5b. Tauc's plot of CNTS thin films at 350° C, 400 °C and 450 °C.

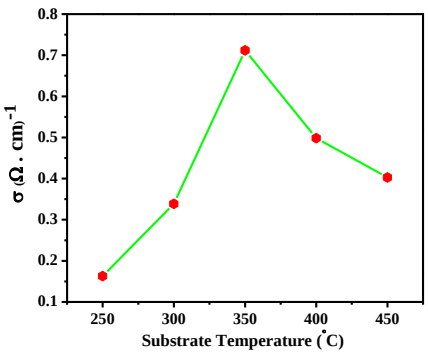

Fig. 6. Variation of Hall conductivity with substrate temperature of CNTS thin films.

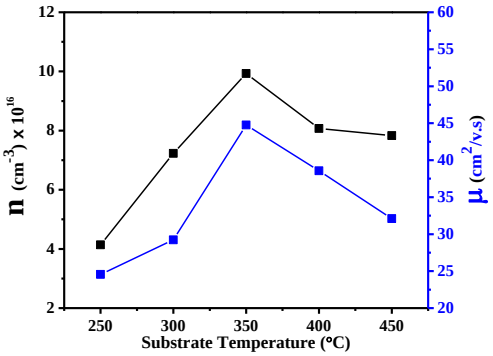

Fig. 7. Variation of charge carriers concentration and mobility with substrate temperature for CNTS thin films.

4. Conclusions

X-ray diffraction measurements of CNTS films that had been deposited on glass substrates at different temperatures of 250, 300, 350, 400, and 450 °C showed that the thin CNTS films were polycrystalline, had a cubic structure and a dominant and preferred growth orientation in the (111) plane. The spectral analysis of the Raman spectroscopy showed a large and distinctive peak at position 336 cm^{-1}, which was attributed to the quadrilateral CNTS compound, confirming the results of the X-ray diffraction. The optical energy gap showed values of 1.57-1.82 eV. This approach determined the ideal energy gap for absorbent materials used in thin-film solar cells. The electrical measurement of the Hall Effect showed that the conductivity was of the p-type.

References

[1] N. Bitri, S. Dridi, F. Chaabouni, M. Abaab, Materials Letters **213**, 31 (2018).
[2] C. L. Yang, Y. H. Chen, M. Lin, S. L. Wu, L. Li, W. C. Liu, X. S. Wu, F. M. Zhang, Materials Letters **166**, 101 (2016).
[3] B. Nabeel A., S. Sabah A., H. Sabreen A., International Journal of Applied Engineering Research **13**(6), 3379 (2018).
[4] J. Akshay, Ch. Tapas K., P. Sanjay, T. Aditi, Kh. Vipul, R. Abhijit, Materials Letters **215**, 118 (2018).
[5] S. Dridi, N. Bitri, and M. Abaab, Materials Letters **204**, 61 (2017).
[6] F. Dahlin, Y. Akhmad H., S. Nofrijon, A. Tri, L. Latifa H., AIP Conference Proceedings **1826**(1), (2017).
[7] M. A. Ahmed, N. A. Bakr, A. A. Kamil, Chalcogenide Letters **16**(5), 231 (2019).
[8] B. G. Sahaya D., S. X. Sahaya, S. Alwin, V. Ramasubbu, B. Gopal M., Journal of Electronic Materials **47**(1), 312 (2018).
[9] G. Anima, Ch. Dhirendra K., B. Amrita, Th. Rajalingam, G. Udayabhanu, RSC Advances **6**(116), 115204 (2016).
[10] B. Reshma K., A. Shruti A., A. Ishita , N. Rounak A., O. Satishchandra, RSC Advances **4**(42), 21989 (2014).
[11] B. Nabeel A., Kh. Ziad T., M. Hussein I., International Journal of Materials Science and Applications **5**(6), 261 (2016).
[12] Ch. Adel, B. Mohamed F., B. Brahim, Journal of Materials Science: Materials in Electronics **30**(4), 3338 (2019).
[13] M. Krishnaiah, M. Sudhanshu, B. Parag, S. Sebastian, K. Talysa R., Maikel F. A. M. van Hest, Journal of Alloys and Compounds **725**, 510 (2017).